Flow Measurement and Instrumentation 31 (2013) 86–95

Contents lists available at SciVerse ScienceDirect

Flow Measurement and Instrumentation

journal homepage: www.elsevier.com/locate/flowmeasinst

Measurement of velocity profiles in multiphase flow using a multi-electrode electromagnetic flow meter

T. Leeungculsatien*, G.P. Lucas

School of Computing and Engineering, University of Huddersfield, Huddersfield HD1 3DH, UK

ARTICLE INFO

Available online 23 October 2012

Keywords:
Velocity profile
Multi-electrode electromagnetic flow meter
Multiphase flow

ABSTRACT

This paper describes an electromagnetic flow meter for velocity profile measurement in single phase and multiphase flows with non-uniform axial velocity profiles. A Helmholtz coil is used to produce a near-uniform magnetic field orthogonal to both the flow direction and the plane of an electrode array mounted on the internal surface of a non-conducting pipe wall. Induced voltages acquired from the electrode array are related to the flow velocity distribution via variables known as 'weight values' which are calculated using finite element software. Matrix inversion is used to calculate the velocity distribution in the flow cross section from the induced voltages measured at the electrode array. This paper presents simulations and experimental results including, firstly the effects of the velocity profile on the electrical potential distribution, secondly the induced voltage distribution at the electrode pair locations, and thirdly the reconstructed velocity profile calculated using the weight values and the matrix inversion method mentioned above. The flow pipe cross-section is divided into a number of pixels and, in the simulations, the mean flow velocity in each of the pixels in single phase flow is calculated from the measured induced voltages. Reference velocity profiles that have been investigated in the simulations include a uniform velocity profile and a linear velocity profile. The results show good agreement between the reconstructed and reference velocity profiles. Experimental results are also presented for the reconstructed velocity profile of the continuous water phase in an inclined solids-in-water multiphase flow for which the axial water velocity distribution is highly non-uniform. The results presented in this paper are most relevant to flows in which variations in the axial flow velocity occur principally in a single direction.

1. Introduction

Conventional electromagnetic flow meters (EMFMs) have previously been used successfully in varieties of industries for measuring volumetric flow rates of conducting fluids in single phase pipe flows. At present, a conventional EMFM can measure the volumetric flow rate of a single phase flow with an error as low as $\pm 0.05\%$ of reading provided that the velocity profile is axisymmetric. However highly non-uniform velocity profiles are often encountered, e.g. just downstream of partially open valves. The axial flow velocity just downstream of a gate valve varies principally in the direction of the valve stem, with the maximum velocities occurring behind the open part of the valve and the minimum velocities behind the closed part of the valve. In such non-uniform velocity profiles the accuracy of the conventional EMFM can be seriously affected [1] but high accuracy volumetric flow rate measurements could be achieved by measuring the axial velocity profile and using this to determine the mean flow velocity in the cross section. Large variations in the axial flow velocity can also occur in multiphase flows e.g. horizontal and upward inclined multiphase flows in which axial velocity variations occur principally in the direction of gravity, with the minimum axial velocity at the lower side of the inclined pipe and the maximum velocity at the upper side of the inclined pipe. A specific example of a multiphase flow which is of great interest to the oil industry is upward inclined oil-in-water flow. Such flows are 'water continuous' and so the multiphase mixture is electrically conducting allowing the use of electromagnetic flow meters. However since the water velocity varies from a minimum at the lower side of the inclined pipe to a maximum at the upper side of the inclined pipe this causes erroneous readings from a conventional electromagnetic flow meter. Another flow of interest to the oil industry occurs during the drilling of inclined oil wells when rock cuttings flow co-currently with water based drilling mud. Mixture density variations in the flow cross section, caused by settling of the rock cuttings, can cause variations in the axial mud velocity from positive (upward) values at the upper side of

* Corresponding author.
E-mail addresses: t.leeungculsatien@hud.ac.uk (T. Leeungculsatien), g.lucas@hud.ac.uk (G.P. Lucas).

0955-5986
http://dx.doi.org/10.1016/j.flowmeasinst.2012.09.002

the inclined well to negative (downward) values at the lower side. In view of the above, the objective of this paper is to describe a new non-intrusive electromagnetic flow metering technique for (i) measuring the axial velocity profile of single phase flows of conducting fluids and (ii) measuring the axial velocity profile of the conducting continuous phase of multiphase mixtures (such as horizontal and inclined oil-in-water flows and solids-in-water flows) in which the conductivity of the dispersed phase is very much lower than the conductivity of the continuous phase. [Note that in a previous paper [2] it has been shown that the relatively minor variations of fluid conductivity, which occur in the cross section of such multiphase flows, have only a minimal effect on the operation of electromagnetic flow meters. This is particularly true if the volume fraction of the non-conducting dispersed phase is less than about 0.4].

An alternative approach to accurate volumetric flow rate measurement in highly non-uniform single phase flows has been proposed by authors such as Horner [3] and Xu et al. [4] who described multi-electrode electromagnetic flow meters which are relatively insensitive to the flow velocity profile. However, this type of flow meter does not provide information on the local axial velocity distribution in the flow cross section. This can be a major drawback, particularly in a steady multiphase flow where, for example, the volumetric flow rate Q_c of a given phase can only be found by integrating the product of the steady local velocity v_c and the steady local volume fraction α_c of the phase in the flow cross section as follows

$$Q_c = \int_A v_c \alpha_c dA \tag{1}$$

where in Eq. (1) A refers to cross sectional area. The approach of Horner [3] would be of no benefit in determining the water volumetric flow rate in a highly inclined oil-in-water flow such as that described above—but in such a flow, the distribution of the local water velocity v_w could be determined using the electromagnetic flow metering method outlined in this paper and the distribution of the local water volume fraction α_w could be obtained non-intrusively using electrical resistance tomography (ERT) [5] enabling the water volumetric flow rate Q_w to be determined according to Eq. (1). Although previous work on velocity profile measurement using multi-electrode electromagnetic flow meters is reported in the literature (see for example [6] for a brief review) much of this previous work is not specifically aimed at multiphase flow measurement which is a major thrust of the work described in this paper. Also much of this previous work involves only simulations rather than the use of a practical device such as that described later in this paper.

The essential theory of electromagnetic flow meters (EMFMs) states that charged particles, in a conducting material which moves in a magnetic field, experience a Lorentz force acting in a direction perpendicular to both the material's motion and the applied magnetic field. Williams [7] applied a uniform transverse magnetic field perpendicular to the line joining the electrodes and the fluid motion and his experiments revealed that for a uniform velocity profile the flow rate is directly proportional to the voltage measured between the two electrodes. Subsequently Shercliff [8] showed that the local current density $\boldsymbol{j}$ in the fluid is governed by Ohm's law in the form of

$$\boldsymbol{j} = \sigma(\boldsymbol{E} + \boldsymbol{v} \times \boldsymbol{B}) \tag{2}$$

where σ is the local fluid conductivity, $\boldsymbol{v}$ is the local fluid velocity, and $\boldsymbol{B}$ is the local magnetic flux density. The expression $(\boldsymbol{v} \times \boldsymbol{B})$ represents the local electric field induced by the fluid motion, whereas $\boldsymbol{E}$ is the electric field due to charges distributed in and around the fluid. For fluids where the conductivity variations are relatively minor (such as the single phase and the multiphase flows under consideration in this paper) Shercliff [8] simplified Eq. (2) to show that the local potential U in the flow can be obtained by solving

$$\nabla^2 U = \nabla \cdot (\boldsymbol{v} \times \boldsymbol{B}) \tag{3}$$

For a circular cross section flow channel bounded by a number of electrodes, with a uniform magnetic field of flux density $\overline{B}$ normal to the axial flow direction, it can shown with reference to [8] that, in a steady flow, the potential difference U_j between the j^{th} pair of electrodes is given by an expression of the form

$$U_j = \frac{2\overline{B}}{\pi a} \iint v(x,y) W(x,y)_j dx dy \tag{4}$$

where $v(x,y)$ is the steady local axial flow velocity at the point (x,y) in the flow cross section, $W(x,y)_j$ is the so-called 'weight value' relating the contribution of $v(x,y)$ to U_j and a is the internal radius of the flow channel. Eq. (4) can be discretized as follows by assuming that the flow cross section can be divided into $\hat{I}$ elemental regions

$$U_j = \frac{2\overline{B}}{\pi a} \sum_{n=1}^{\hat{I}} \hat{v}_n \hat{W}_{n,j} \hat{A}_n \tag{5}$$

where $\hat{v}_n$ and $\hat{A}_n$ are respectively the local axial velocity in, and the cross sectional area of, the nth elemental region. $\hat{W}_{n,j}$ is the weight value describing the contribution of the axial velocity in the nth elemental region to the jth potential difference U_j. If the axial flow velocity is now assumed to be constant in each of N large regions, Eq. (5) can be written as

$$U_j = \frac{2\overline{B}}{\pi a} \sum_{i=1}^{N} v_i \sum_{n=\hat{I}_{i-1}+1}^{\hat{I}_i} \hat{W}_{n,j} \hat{A}_n \tag{6}$$

where v_i is the axial flow velocity in the ith large region. In Eq. (6) when the subscript n is in the range $\hat{I}_{i-1}+1 \le n \le \hat{I}_i$ it refers to the elemental regions lying within the ith large region. [Note also that there are $\hat{I}_i - \hat{I}_{i-1}$ elemental regions within the ith large region and that, by definition, $\hat{I}_0 = 0$]. An 'area weighted' mean weight value w_{ij} relating the contribution of the velocity v_i in the ith large region to the jth potential difference U_j is given by

$$w_{ij} = \frac{\sum_{n=\hat{I}_{i-1}+1}^{\hat{I}_i} \hat{W}_{n,j} \hat{A}_n}{A_i} \tag{7}$$

where A_i is the cross sectional area of the ith large region. Combining Eqs. (6) and (7) gives

$$U_j = \frac{2\overline{B}}{\pi a} \sum_{i=1}^{N} v_i w_{ij} A_i \tag{8}$$

It will be shown later in this paper that Eq. (8) can be inverted to enable estimates of the local axial flow velocity v_i in each of N large pixels to be determined from N potential difference measurements U_j made on the boundary of the flow. Furthermore, although Eq. (8) was derived on the assumption that the axial velocity in each large pixel is constant, it will be seen that when this inversion method is used to solve for the velocity in each large pixel then the values of v_i obtained give a good approximation to the mean axial velocity in each of the large pixels, in situations where there is some axial velocity variation within each large pixel.

In Section 2 of this paper it is shown how the weight values w_{ij} can be calculated, for a particular magnetic flow meter geometry, using finite element techniques. In Section 3 values of U_j are calculated for a number of different simulated velocity profiles in the EMFM. In Section 4 of the paper, a reconstruction technique is outlined which enables the pixel velocities v_i to be determined from the weight values w_{ij} and the boundary voltage measurements U_j. In Section 5 a practical EMFM is presented and in Section 6 results

obtained from this practical EMFM device in a multiphase flow are presented.

2. Numerical modeling of the electromagnetic flowmeter

2.1. Electromagnetic flow meter geometry

In order to calculate the weight values w_{ij} it is necessary to use finite element techniques to solve Eq. (2) to determine the potential distribution within the electromagnetic flow meter for a variety of different flow velocity profiles (see Section 2.3). It was decided to use the COMSOL [9] finite element solver to do this because its software also enables prediction of the magnetic field produced by the electromagnetic flow meter's Helmholtz coil. The specification of the EMFM was that it consisted of a PTFE (polytetrafluoroethylene) flow pipe mounted within a Helmholtz coil. The EMFM contained 16 equispaced electrodes located at the plane $z=0$, which was also the plane containing the centers of the 2 coils forming the Helmholtz coil. The inner diameter of the flow pipe was 0.08 m, the outer diameter was 0.09 m and its axial length was 0.3 m. The inner and outer diameters of the two coils forming the Helmholtz coil were 0.2048 m and 0.2550 m respectively (refer to Fig. 1(a)). A cylindrical domain with a diameter of 0.32 m and a length of 0.32 m represented the boundary of the computing domain (Fig. 1). The boundary condition for the simulations was that the component of the magnetic field normal to the boundary of the computing domain was set to zero.

In order to calculate the relevant weight values (see Section 1) potential difference measurements must be acquired from electrode pairs at the internal boundary of the flow pipe (at the plane $z=0$), these electrodes being in contact with the flowing medium. Sixteen electrodes were placed at angular intervals of 22.5 degrees on the flow pipe boundary (refer to Fig. 2) the electrodes being denoted e1, e2 etc, with electrode e5 at the top of the flow cross section and electrode e13 at the bottom of the flow cross section (Fig. 2). For the simple flow meter geometry described in this paper the flow cross section was divided into seven pixels. The geometry of these seven pixels was chosen such that the chords joining seven pairs of electrodes were located at the geometric centers (in the y direction) of the pixels (refer to Fig. 2). The fluid pixels are categorized as pixel 1 at the top of the flow cross section to pixel 7 at the bottom of the flow cross section. This pixel arrangement was chosen because, as described in Section 1, variations in the axial velocity in many flows of interest tend to occur in a single direction. Thus, for measuring the velocity profile behind a partially open gate valve, the flow meter would be orientated such that the line joining e13 to e5 would be parallel to the valve stem (i.e. the direction of the magnetic field would be parallel to the valve stem). For making measurements in horizontal or inclined oil-in-water flows the line joining e13 to e5 would be in the direction from the uppermost side of the pipe to the lowermost side. The pixel areas A_i are shown in Table 1. In the simulations described in this paper, for each simulated flow condition investigated, potential difference measurements were made between the seven electrode pairs shown in Table 1 (the jth potential difference measurement U_j was made between the jth electrode pair shown in Table 1). At the plane of the electrodes, where $z=0$, the local magnetic flux density $\boldsymbol{B}$ was always perpendicular to both the fluid flow direction and to the chords joining the electrode pairs (i.e. it was in the y direction shown in Figs. 1 and 2). The fluid

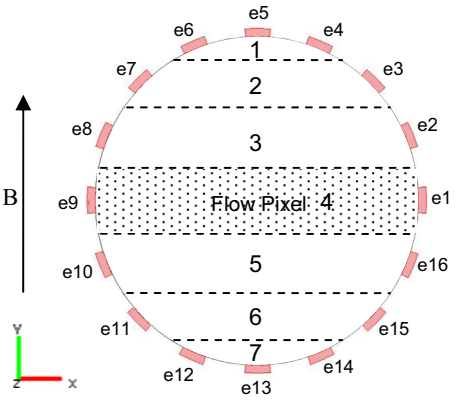

Fig. 2. Schematic diagram of the flow pixels, the electrodes and the direction of the magnetic field.

Table 1
Electromagnetic flow meter geometries.

Area A_i (m^2)		Electrode pair Uj	
(a) Pixel areas		(b) Electrode pair	
Pixel1 ($i=1$)	$1.738\ e^{-4}$	Pair 1 ($j=1$)	e4–e6
Pixel2 ($i=2$)	$6.267\ e^{-4}$	Pair 2 ($j=2$)	e3–e7
Pixel3 ($i=3$)	$1.077\ e^{-3}$	Pair 3 ($j=3$)	e2–e8
Pixel4 ($i=4$)	$1.264\ e^{-3}$	Pair 4 ($j=4$)	e1–e9
Pixel5 ($i=5$)	$1.077\ e^{-3}$	Pair 5 ($j=5$)	e16–e10
Pixel6 ($i=6$)	$6.267\ e^{-4}$	Pair 6 ($j=6$)	e15–e11
Pixel7 ($i=7$)	$1.738\ e^{-4}$	Pair 7 ($j=7$)	e14–e12

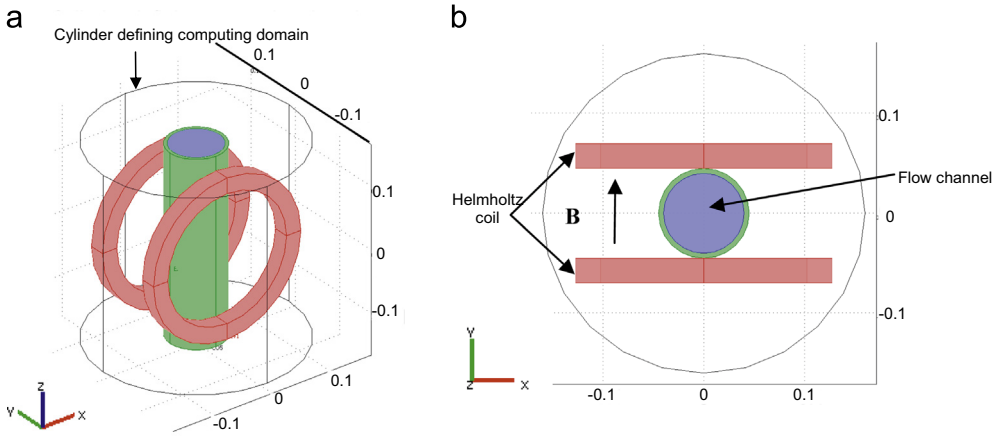

Fig. 1. Schematic diagram of the electromagnetic flow meter used in the simulation. (a) 3D view and (b) View on x –y plane.

conductivity used in the simulations was$1.5\times10^{-2}\,\mathrm{Sm}^{-1}$ this conductivity value being typical of the mains water in the Huddersfield region of Northern England where the experiments described in Section 6 were carried out. In addition the flow pipe was assumed to be made of PTFE with conductivity of $1\times10^{-15}\,\mathrm{Sm}^{-1}$, and the Helmholtz coil material was assumed to be copper with a conductivity of $5.96\times10^{7}\,\mathrm{Sm}^{-1}$.

[Note that for a sixteen electrode system, such as that shown in Fig. 2, up to fifteen independent potential difference measurements could be made. With reference to the techniques described in Sections 1 and 4 of this paper, this would allow the flow velocity to be determined in up to 15 pixels into which the flow cross section could be divided. The sizes and shapes of these 15 pixels could be selected as required (provided that the relevant weight functions relating the pixel velocities to the boundary potential difference measurements are calculated). If the variation of the axial velocity was unlikely to be in a single direction then instead of using the pixel arrangement shown in Fig. 2, the use of pixels of approximately square shape would be more appropriate. Note also that although in the study described in this paper electrodes e13 and e5 are not used, they would be required if additional pixels were used as described above].

2.2. Simulated magnetic flux density distribution

In the present investigation a Helmholtz coil was used to produce a near uniform local magnetic flux density distribution in the flow cross section. COMSOL finite element software [9] enabled simulation of the distribution of the magnetic flux density $\boldsymbol{B}$ in the computing domain produced by this Helmholtz coil. The Helmholtz coil consisted of two identical circular coils placed symmetrically on each side of the PTFE flow pipe as shown in Fig. 1. The coils were simulated such that electrical current flowed through both coils in the same direction and each coil carried the same current density. In the simulations described in this section, the current density in each coil was set such that the mean magnetic flux density in the y direction (see Figs. 1 and 2) was 110.4 G (110.4×10^{-4} T) in the flow cross section at the plane of the electrodes (where $z=0$). This was similar to the value of the mean magnetic flux density in the y direction required for the practical electromagnetic flow meter described in Section 5. In the simulations, for this mean value of the magnetic flux density, the minimum and maximum values of the magnetic flux density in the y direction in the flow cross section at the plane $z=0$ were 109 G and 112 G respectively, showing that the magnetic field was very close to being uniform in the flow cross section.

2.3. Calculation of the weight values

To numerically simulate the weight values w_{ij}, relating the mean flow velocity v_i in the ith pixel to the jth potential difference measurement U_j between the jth pair of electrodes on the flow boundary, the flow channel is divided into seven pixels as described above (refer to Fig. 2). The fluid in the pixel for which weight values are to be calculated is given an axial flow velocity (in the z direction) greater than zero whilst the remaining pixels all have zero fluid velocity. The COMSOL finite element solver is then used to determine the distribution of the electrical potential U in the computing domain, for the magnetic flux density distribution in the flow cross section, at the plane $z=0$, as given in Section 2.2 above. [Note that for this finite element simulation of the electrical potential distribution, the number of mesh elements in the flow cross section at the plane $z=0$ was 488]. Fig. 3 shows the distribution of the Lorentz forces and the induced electrical potentials when the fluid in pixel 4 has an imposed velocity in the z direction while the fluid in the remaining pixels is at rest. Fig. 3(a) illustrates the Lorentz force distribution arising from the imposed velocity in pixel 4. The magnetic field interacts with the charges carried in the water via these Lorentz forces causing the separation of charged ions (positive and negative) and giving rise to the electrical potential distribution shown in Fig. 3(b). The arrows shown in Fig. 3(a) also represent the direction of the local induced current density and it can be seen that for the (highly contrived) case in which flow occurs in pixel 4 only there is circulation of the electric current.

From the calculated potential distribution on the boundary of the flow (see also Fig. 3(b)) the seven potential differences U_j between the 7 electrode pairs given in Table 1 can be calculated allowing all of the weight values w_{4j} associated with pixel 4 to be calculated according to Eq. (9) (with $i=4$ and $j=1$–7). The process is then repeated for each of the other six pixels in succession until all relevant 49 weight values have been calculated. Fig. 4(a) shows the induced voltages plotted against electrode pairs for all of the seven simulations. Fig. 4(b) shows the 49 weight values calculated from the induced voltages given in Fig. 4(a) by using Eq. (9).

$$w_{ij}=U_j\frac{\pi a}{2\overline{B}}\frac{1}{v_iA_i} \tag{9}$$

Note that the values of w_{ij} calculated according to Eq. (9) are independent of the value of v_i used in the simulation because, for given values of i and j, U_j is proportional to v_i. The weight values w_{ij} calculated using Eq. (9) are equivalent to the values of w_{ij} that would be obtained using Eq. (7). [NB: For a more detailed account of the application of the weight value technique to electromagnetic flow metering the interested reader is referred to the seminal work

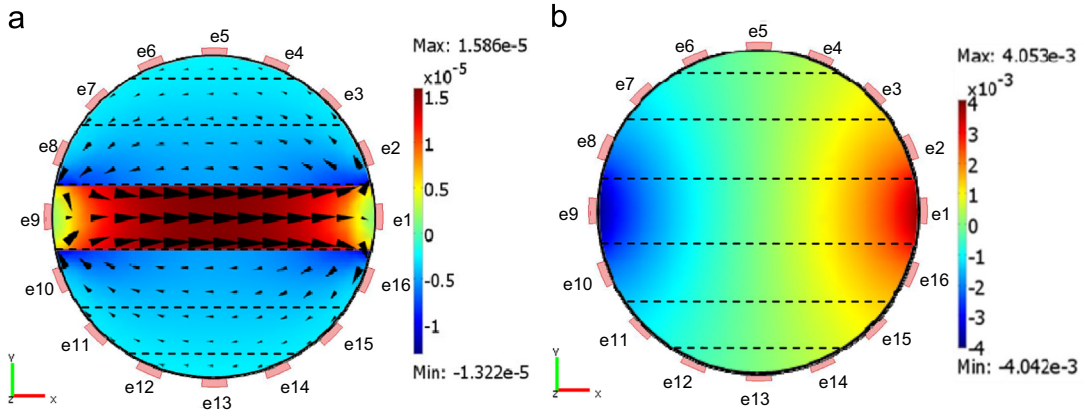

Fig. 3. (a) Simulation of Lorentz force distribution per unit volume [N/m^3] when flow is imposed in pixel 4 only (the arrows may also be taken as an indication of the magnitude and direction of induced electrical current). (b) Simulated distribution of induced electrical potential [V] on z plane when flow is imposed in pixel 4 only.

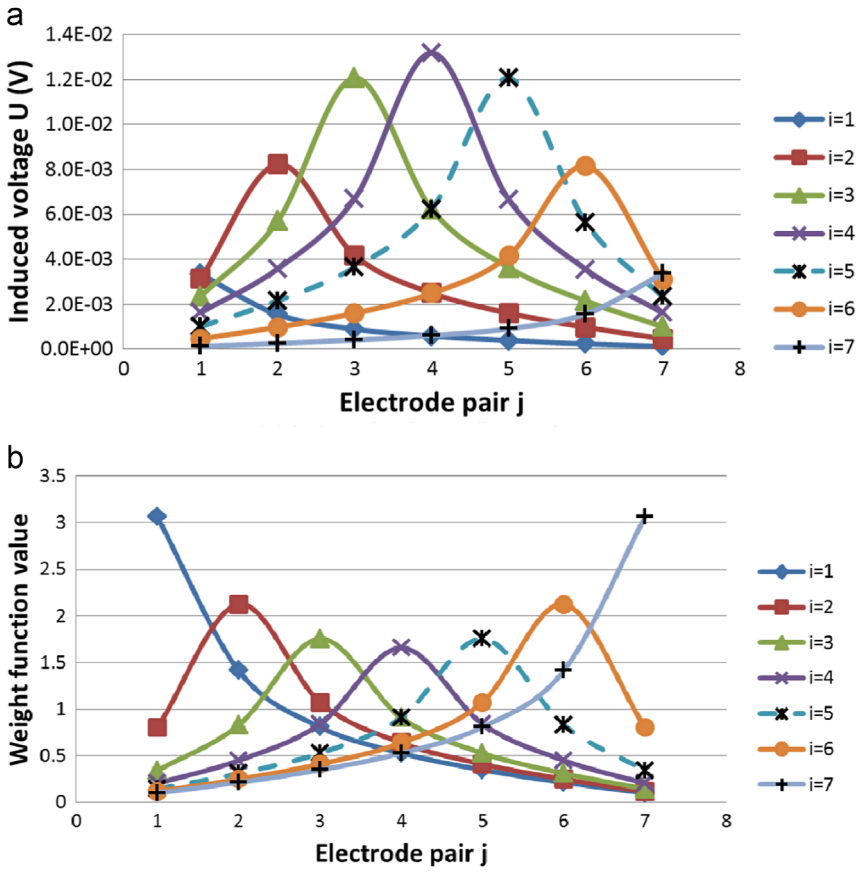

Fig. 4. (a) Simulation results for the induced voltage between the j'th electrode pair when flow occurs only in the i'th pixel; and (b) resultant weight values relating the voltage between the j'th electrode pair to the velocity in the i'th pixel.

of Shercliff [8]]. It is worth noting, with reference to [8], that if 'point' electrodes are assumed, then the local weight value $W(x,y)_j$ (see Section 1) at the precise position of a point electrode can sometimes be analytically calculated to be infinite. Eqs. (4)–(7) indicate that an infinite local value of $W(x,y)_j$ should cause some of the w_{ij} values to be infinite. Since the mesh elements used in the simulations were of finite size it is unlikely that infinite values of w_{ij} would have been observed, nevertheless the facts that (i) not even exceptionally large values of w_{ij} were observed in the simulations; and (ii) the calculated values of w_{ij} enabled accurate velocity profile reconstruction to be performed (see Sections 4 and 6), suggest that infinite weight values $W(x,y)_j$ that can be obtained analytically are of little practical significance—almost certainly because they act over an infinitesimally small region of the flow.

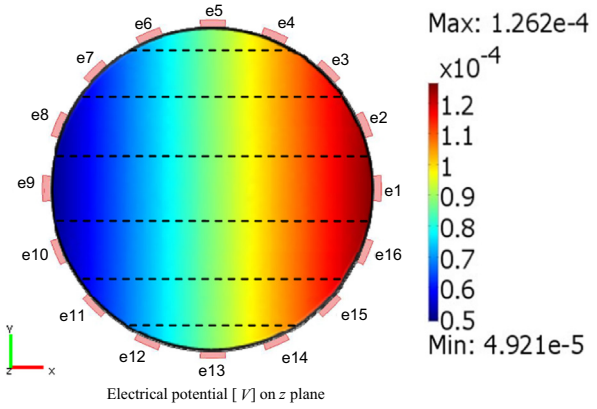

Fig. 5. Simulated induced potential distribution for a uniform velocity profile of 2 ms^{-1}.

3. Effect of velocity profile on electrical potential distribution

The next stages of the investigation were; (i) to apply different simulated velocity profiles to a flowing single phase fluid (water); (ii) to find the resultant induced potential differences U_j using COMSOL; (iii) to reconstruct the single phase velocity profiles (see Section 4); and (iv) to compare the reconstructed velocity profiles with the applied simulated velocity profiles. Two different simulated velocity profiles were investigated, a uniform velocity distribution and a linear velocity distribution as described below.

3.1. Uniform velocity profile

Fig. 5 shows the potential distribution arising from an imposed uniform, single phase (water), velocity distribution of 2 ms^{-1} in the flow cross section. The authors acknowledge that this velocity profile is unrealistic because fully developed, turbulent, single phase flows in circular pipes are generally axisymmetric with '1/7th power law' velocity profiles. Nevertheless, as a means of investigating flow velocity image reconstruction techniques this uniform velocity profile is very useful in its simplicity.

3.2. Linear velocity profile

Fig. 6 shows the potential distribution arising from an imposed, linear single phase (water) velocity distribution in the flow cross section. The axial flow velocity v_z in the z direction is given by the

expression

$$v_z = 1 + \left(\frac{y}{a}\right) \tag{10}$$

where y is the coordinate in the simulation in the direction shown in Fig. 6 and a is the internal pipe radius. This results in v_z varying linearly from zero at $y=-0.04$ m to 2 ms^{-1} at $y=0.04$ m. This type of linearly varying velocity profile has previously been reported in [10] (albeit for multiphase rather than single phase flows).

The relevant induced voltages U_j for the uniform velocity profile and linear velocity profile were calculated for the electrode pairs shown in Table 1. It should be noted that the electrical potential distribution for the uniform velocity profile and linear velocity profile are entirely different from each other. For the uniform velocity distribution the induced voltages between pairs 1, 2 and 3 are the same as for pairs 7, 6, and 5 are respectively. For the linear velocity profile the induced voltage between pair 1 is higher than that for pair 7. Similarly the induced voltages between pairs 2 and 3 are respectively higher than for pairs 6 and 5. Moreover for the linear velocity profile the highest induced voltage is between electrode pair 3 while the maximum induced voltage for the uniform velocity profile is between electrode pair 4. Similar relationships between the velocity profile and the induced voltage distribution have also been previously observed [2].

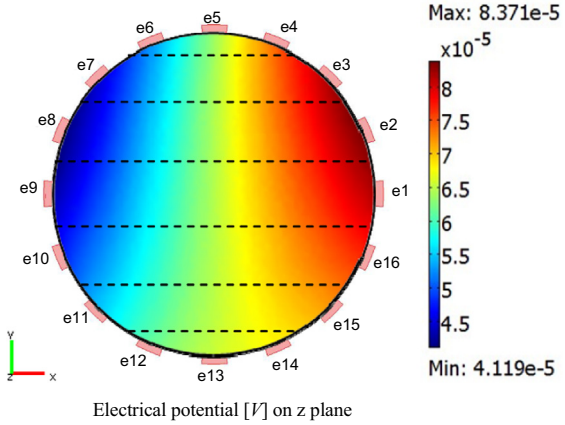

Fig. 6. Simulated induced potential distribution for the axial flow velocity varying linearly from 0 ms^{-1} at $y=-0.04$ m to 2 ms^{-1} at $y=+0.04$ m.

4. Simulated velocity profile reconstruction

As mentioned earlier, the weight values w_{ij} are used to reconstruct the mean velocity v_i in each pixel using the calculated induced voltages U_j. The reconstruction method can be expressed simply by the following matrix equation

$$\boldsymbol{V} = \frac{\pi a}{2B}[\boldsymbol{WA}]^{-1}\boldsymbol{U} \tag{11}$$

In which $\boldsymbol{V}$ is a single column matrix containing the pixel velocities v_i, $\boldsymbol{W}$ is a square matrix containing the relevant weight values w_{ij}, $\boldsymbol{A}$ is a diagonal matrix containing information on the pixel areas A_i and $\boldsymbol{U}$ is a single column matrix containing the calculated potential differences U_j for a given imposed velocity profile. The inversion of $[\boldsymbol{WA}]$ was performed using a Tikhonov regularization technique involving singular value decomposition (SVD) of $[\boldsymbol{WA}]$ (see for example [6]).

For the two velocity profile simulations that were undertaken the reconstructed velocity profiles are shown in Fig. 7(a) and (b). Also shown in Fig. 7(a) and (b) are the original imposed velocity profiles (which show the mean imposed flow velocity in each pixel) from which the potential difference measurements U_j were obtained. With close inspection of Fig. 7 it can be seen that the reconstructed velocity profiles have reasonable agreement with the original imposed velocity profiles for both the uniform and linear velocity profiles. Fig. 7(a) shows that for the imposed uniform, single phase (water) velocity profile the maximum (most overestimated) and minimum (most under estimated) reconstruction errors occur in pixel 1 (+3.23%) and pixel 5 (−2.31%) respectively. The most accurate reconstructed velocity is in pixel 6 with an error of only 0.5%. The linear, single phase (water) velocity profile has maximum and minimum reconstruction errors in pixels 1 and 7 respectively. The most accurate reconstructed velocities for the linear velocity profile are in pixels 3 and 6 with errors of −0.99%and −0.24% respectively. The errors in the reconstructed linear velocity profile may be due to violation of the assumption in Eq. (6) that the flow velocity is constant in a given pixel. Nevertheless, despite this violation, the imposed linear profile can be seen to be reconstructed with reasonably good accuracy.

[Note that, as stated in Section 2.1, for a 16 electrode system (such as that used in the present study) it is possible to make 15 independent potential difference measurements U_j, and so it would actually be possible to divide the flow cross section into 15 rather than 7 pixels. It might be thought that a 15 pixel system would enable a more accurate reconstructed velocity profile to be obtained. However the accuracy of the velocity reconstruction method is highly dependent upon the condition number of the matrix $[\boldsymbol{WA}]$

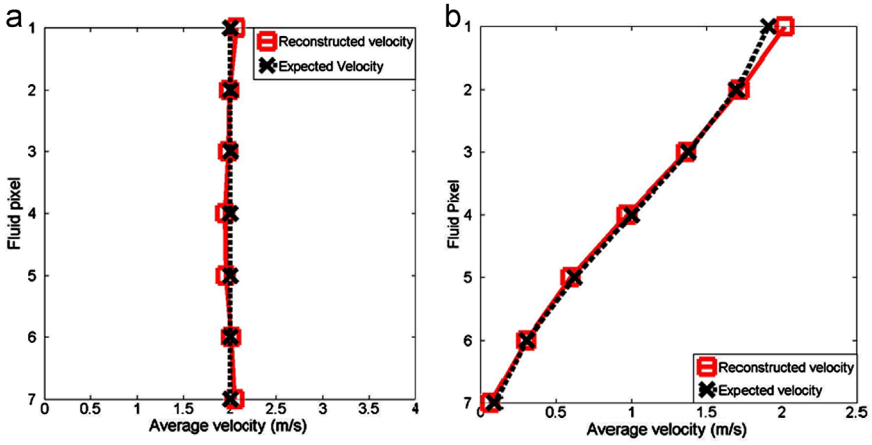

Fig. 7. Imposed (squares) and reconstructed (crosses) velocity profiles. (a) Reconstructed uniform velocity profile and (b) Reconstructed linear velocity profile.

and this condition number rises rapidly as the number of pixels is increased, making the technique more susceptible to measurement errors in U_j. For the 7 pixel arrangement shown in Fig. 2 the condition number of [***WA***] is 8.4, but for a typical 15 pixel arrangement the condition number rises to about 130,000. Fig. 2 represents an optimum arrangement, giving the maximum number of pixels for which the condition number of [***WA***] is acceptably small].

The total volumetric flow rate Q_w of the water can be calculated from a reconstructed velocity profile as follows;

$$Q_w = \sum_{i=1}^{7} A_i v_i \tag{12}$$

where A_i is the area of the ith pixel, and v_i is the reconstructed velocity in the ith pixel. Let the true volumetric flow rate associated with the imposed uniform velocity profile be Q_{wiu} and the volumetric flow rate associated with the reconstructed uniform velocity profile be Q_{wru}. Also let the true volumetric flow rate associated with the imposed linear velocity profile be Q_{wil} and the volumetric flow rate associated with the reconstructed linear velocity profile be Q_{wrl}. For the uniform velocity profile Q_{wiu} is calculated to be 36.13 $m^3\,hr^{-1}$ and Q_{wru} is found to be 35.71 $m^3\,hr^{-1}$. There is thus an error of only -1.17% in the total volumetric flow rate obtained from the reconstructed uniform velocity profile. For the linear velocity profile Q_{wil} is calculated to be 18.06 $m^3\,hr^{-1}$, and Q_{wrl} is calculated to be 17.9 $m^3\,hr^{-1}$. There is thus an error of only -0.88% in the total volumetric flow rate obtained from the reconstructed linear velocity profile.

5. A practical electromagnetic flowmetering device

A real imaging electromagnetic flow meter (see Fig. 8) was constructed using the same geometry modeled in the COMSOL simulations described above. The non-conducting flow meter body, with an internal radius of 80 mm, was made from Delrin. Four grooves on the flow meter body were machined to accommodate two circular coils which formed a Helmholtz coil, with the mean spacing between the two coils being equal to the mean coil radius. The electrode array contained 16 electrodes for measuring flow induced potential differences, with each electrode being made from stainless steel. Stainless steel was chosen because (i) it has high corrosion resistance and (ii) it has a low relative permeability which meant that the electrodes did not significantly affect the magnetic field in the flow cross section. Supports (labeled 'E' in Fig. 8) were used to position the cables running between the electrodes and the detection circuitry in such a way that they were always parallel to the local magnetic field. This meant that any 'cable loops' were not cut by the time varying magnetic field—thus preventing non-flow-related potentials from being induced in the cables.

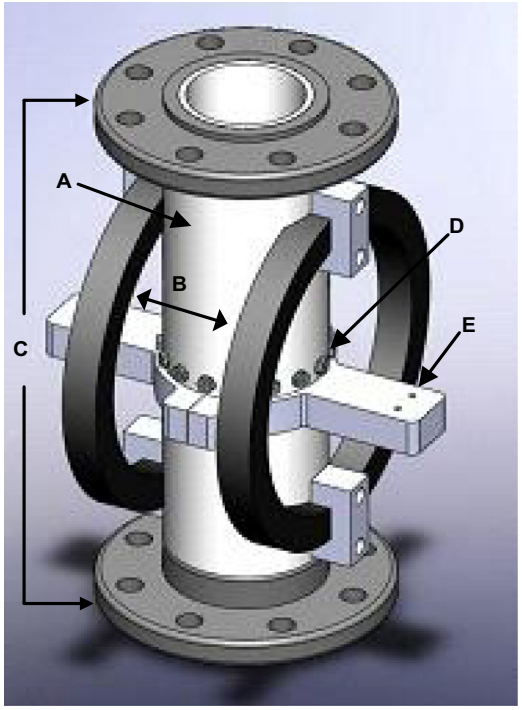

Fig. 8. Design of the electromagnetic flow meter used in the present study.

The technique described in this paper for measuring pixel flow velocities relies upon the magnetic flux density being uniform in the y direction (see Fig. 1) in the flow cross section at the plane of the electrodes. To check the uniformity of the magnetic field produced by the Helmholtz coil a 48 V dc power supply was connected to the two coils which were configured in parallel so that an equal current of 1.372 A flowed in the same direction in each coil. A 'Hirst GM08 G-meter' was then used to measure the magnetic flux density in the y direction at 179 points in the flow cross section at the plane of the electrodes. The results, which are presented graphically in Fig. 9, were analyzed to show that the mean measured magnetic flux density in the flow cross section was 107.33 G, whilst the maximum and minimum measured values of the magnetic flux density were 107.89 G and 106.52 G, indicating the very near uniformity of the magnetic field strength.

In normal operation, all measurement and control operations associated with the EMFM were made using a microcontroller. Furthermore, the flow induced voltage between the jth electrode pair was measured using the circuit shown in Fig. 10 which consisted of two voltage followers and a differential instrumentation amplifier with a gain of 996. A high pass filter was placed after each voltage follower to remove unwanted dc signals. A low

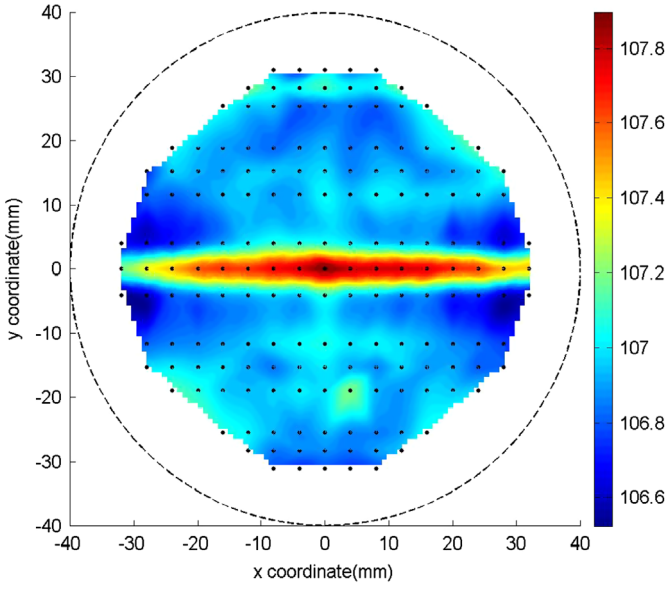

Fig. 9. Distribution of the y-component of the magnetic flux density (gauss) in the flow cross section at the plane of the electrodes. The dashed circular line represents the internal pipe diameter. [NB: Measurements could not be obtained at distances greater than 31.1 mm from the pipe center due to the size of the Gaussmeter sensing head].

pass filter was placed after the differential amplifier to remove high frequency noise. In the present study, seven such circuits were required, one for each electrode pair.

A 'hybrid square wave' magnetic field was generated by switching the voltage supplied to the coils, from the 48 V dc power supply unit, using control signals supplied to a solid-state relay network. At any instant in time, the electrical current in both coils had the same magnitude and direction. Fig. 11a is a schematic of the variation of the mean magnetic flux density $\overline{B}$ in the flow cross section with time for this 'hybrid square wave', the purpose of which was to periodically reverse the direction of the flow induced potential at each electrode, thereby minimizing electrochemical effects at the electrode-water interface. The typical length of each cycle of the 'hybrid square wave' magnetic field used in the present investigation was 0.25 s and the maximum $(+\overline{B}_{\max})$ and minimum $(-\overline{B}_{\max})$ values of the mean magnetic flux density in the flow cross section (in the y direction) were +107.33 G and −107.33 G respectively. The transient time τ_c in the magnetic field, visible in Fig. 11a, was caused by a transient in the current in each coil (when the coil voltage was switched) due to the coil inductance.

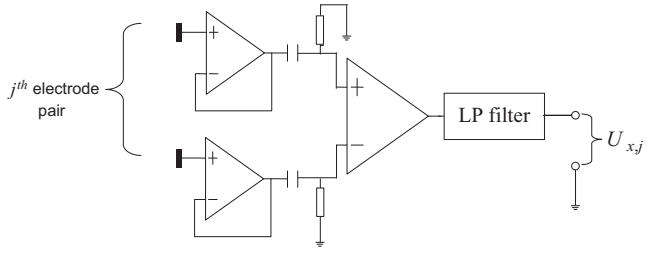

Fig. 10. Electronic circuitry for measuring the flow induced potential difference between each electrode pair.

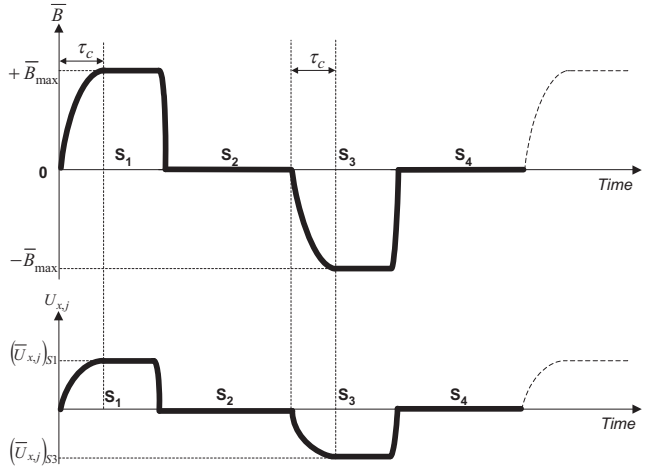

Fig. 11. (a) (top) Hybrid square wave magnetic field cycle. (b) (bottom) resultant flow induced potential difference for jth electrode pair.

Each cycle of the hybrid square wave magnetic field can be divided into four segments, denoted S_1–S_4 in Fig. 11a. Fig. 11b shows one cycle of the jth flow induced voltage signal $U_{x,j}$ between the jth pair of electrodes in the electrode array. For a given magnetic field cycle, mean values $(\overline{U}_{x,j})_{S1}$, $(\overline{U}_{x,j})_{S2}$, $(\overline{U}_{x,j})_{S3}$, and $(\overline{U}_{x,j})_{S4}$ were obtained from measurements of $U_{x,j}$ for each of the four signal segments S_1 to S_4. Note that $(\overline{U}_{x,j})_{S1}$, $(\overline{U}_{x,j})_{S2}$, $(\overline{U}_{x,j})_{S3}$ and $(\overline{U}_{x,j})_{S4}$ were obtained from measurements of $U_{x,j}$ made after the relevant transient (of length τ_c for S_1 and S_3) was complete. For a given magnetic field cycle, the relevant flow induced potential difference U_j required for the pixel velocity calculation (Section 4 and Eq. (11)) was obtained from the average of the difference between the jth measured voltages when $\overline{B} = +\overline{B}_{\max}$ and $\overline{B} = 0$ and the difference between the jth measured voltages when $\overline{B} = 0$ and $\overline{B} = -\overline{B}_{\max}$ as shown in Eq. (13) below. Division by 996 is required in Eq. (13) to compensate for the amplification of the differential instrumentation amplifier described above.

$$U_j = \frac{|(\overline{U}_{x,j})_{s1} - (\overline{U}_{x,j})_{s2}| + |(\overline{U}_{x,j})_{s3} - (\overline{U}_{x,j})_{s4}|}{2} \times \left\{\frac{1}{996}\right\} \tag{13}$$

6. Experimental results in multiphase flow

Measurements of the local water velocity profile in a solids-in-water flow were made using the EMFM device described in Section 5. The experiments were performed in the 3 m long 80 mm internal diameter working section of a multiphase flow loop at the University of Huddersfield (see [10] for a more complete description of the flow loop). For the experiments described in this paper the working section was either vertical ($\theta = 0°$) or inclined at an angle of 30° ($\theta = 30°$) away from vertical. Electrically non-conducting spherical, plastic beads with an average diameter of 4 mm and a density of 1340.8 kgm^{-3} were homogenously mixed with water in a holding tank before being pumped to the base of the working section. The flow rate of the multiphase mixture was controlled by varying the speed of a multiphase pump located between the holding tank and the working section. The EMFM device described in Section 5 was installed 2 m away from the inlet of the working section. At each flow condition, voltages $U_{x,j}$ (j=1 to 7) (see Fig. 10) were measured for the relevant electrode pairs over a period of 60 s (with reference to Section 5, this meant that values of $(\overline{U}_{x,j})_{S1}$, $(\overline{U}_{x,j})_{S2}$, $(\overline{U}_{x,j})_{S3}$ and $(\overline{U}_{x,j})_{S4}$ were obtained from averaging data from 240 magnetic field cycles, since each magnetic field cycle

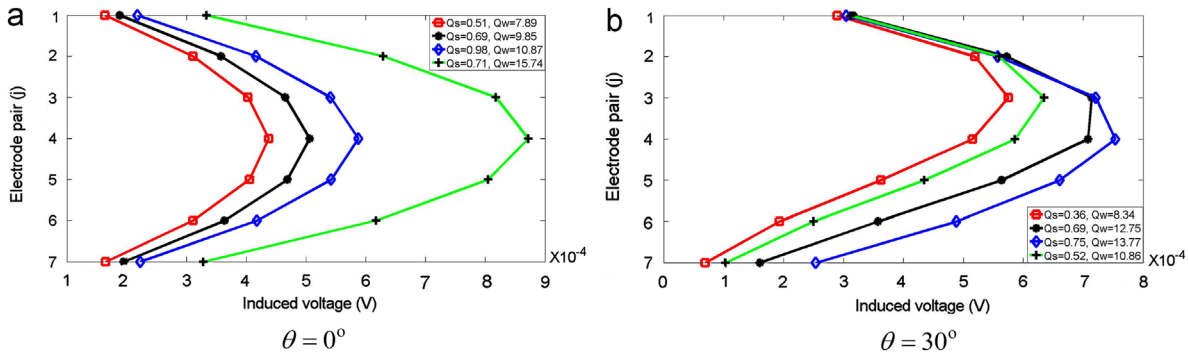

Fig. 12. Flow induced potential differences U_j for (a) vertical and (b) inclined solids-in-water flows.

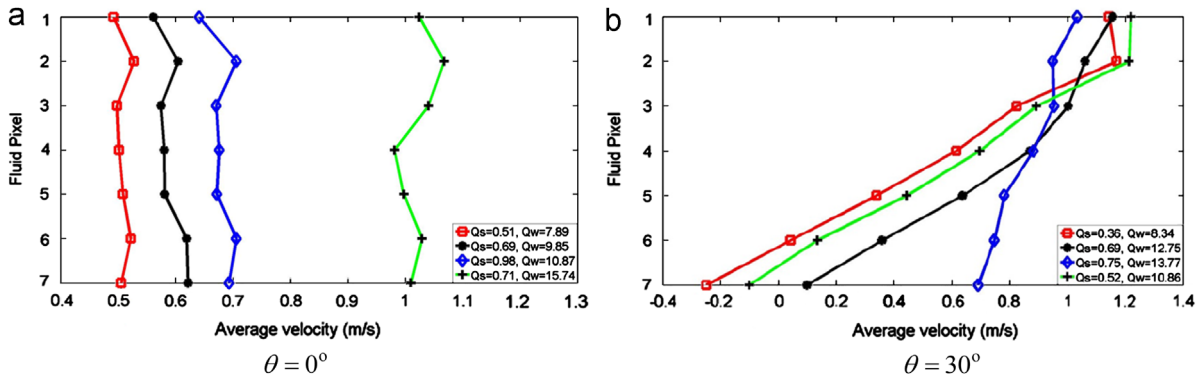

Fig. 13. Reconstructed pixel velocities v_i for (a) vertical and (b) inclined solids-in-water flow.

has a period of 0.25 s). Results for several multiphase flow conditions are presented in Figs. 12 and 13. In these figures, for $\theta=0^\circ$, the solids volumetric flow rate Q_s was in the range 0.51 $m^3\ hr^{-1}$ to 0.98 $m^3\ hr^{-1}$ and the water volumetric flow rate Q_w was in the range 7.89 $m^3\ hr^{-1}$ to 15.74 $m^3\ hr^{-1}$. For $\theta=30^\circ$, Q_s was in the range 0.36 $m^3\ hr^{-1}$ to 0.75 $m^3\ hr^{-1}$ and Q_w was in the range 8.34 $m^3\ hr^{-1}$ to 13.77 $m^3\ hr^{-1}$. These values of Q_s and Q_w are typical of those encountered in industrial slurry monitoring application in 80 mm diameter pipes.

For each flow condition investigated, the induced voltages U_j ($j=1$ to 7) were calculated from the measured values of $(\overline{U}_{x,j})_{S1}$, $(\overline{U}_{x,j})_{S2}$,$(\overline{U}_{x,j})_{S3}$ and $(\overline{U}_{x,j})_{S4}$ according to Eq. (13) and the corresponding pixel velocities v_i ($i=1$ to 7) were then calculated from these values of U_j according to Eq. (11). The values of w_{ij} used in calculating these pixel velocities were those presented in Fig. 4b. Fig. 12 shows a plot of the values of U_j for each electrode pair (refer to Table 1) for all of the flow conditions investigated. Fig. 13 shows a plot of the reconstructed pixel velocities for all of the flow conditions investigated.

The reconstructed velocity profiles illustrated in Fig. 13(b) clearly indicate evidence of negative axial water velocity at the lower side of the inclined pipe, showing that in the seventh pixel, the water was flowing back down the pipe. Towards the upper side of the inclined pipe, the mean axial water velocity was large and positive indicating that the water was flowing quickly upward. These results agree well with visual observation of the flow undertaken using high speed filming. Previous research (e.g. [10]) has reported similar phenomena in inclined solids-in-water flows from results obtained using an intrusive six electrode local conductance velocity measurement probe. Fig. 13(a) shows that for vertical solids-in-water flows the water velocity is much more uniform in the flow cross section. Note that the relatively uniform velocity profiles shown in Fig. 13(a) are typical of the velocity profiles that are seen over a much wider range of vertical solids-in-water flow conditions. Note also that the velocity profiles shown in Fig. 13(b) cover the extremes of velocity profile shape encountered in many inclined (and other stratified) solids in water flows namely (i) relatively minor variations in velocity from pixel 7 to pixel 1, for $Q_s=0.75\ m^3\ hr^{-1}$ and $Q_w=13.77\ m^3\ hr^{-1}$ to (ii) marked backflow in pixel 7 to strong up-flow in pixel 1, for $Q_s=0.36\ m^3\ hr^{-1}$ and $Q_w=8.34\ m^3\ hr^{-1}$.

With reference to Eq. (1), if the local solids and water volume fraction distributions were known (for example by using Electrical Resistance Tomography (see [5] and [10])) then an estimate $Q_{w,est}$ of the water volumetric flow rate could be given by

$$Q_{w,est}=\sum_{i=1}^{7} v_i\alpha_{w,i}A_i \tag{14}$$

where $\alpha_{w,i}$ is the mean water volume fraction in the ith pixel and A_i is the cross sectional area of the ith pixel. If the simplifying assumption is made that there is only very small *local* slip between the phases an estimate $Q_{s,est}$ of the solids volumetric flow rate could be given by

$$Q_{s,est}=\sum_{i=1}^{7} v_i\alpha_{s,i}A_i \tag{15}$$

where $\alpha_{s,i}$ is the mean solids volume fraction in the i^{th} pixel.

7. Conclusions

This paper describes a measurement technique for mapping velocity profiles in single phase and multiphase flows. The results described in this paper are mainly relevant to flows in which the axial flow velocity varies *principally* in a single direction such as (i) flows behind partially open valves or (ii) horizontal and inclined multiphase flows in which the continuous phase is electrically conducting. However by using alternative pixel arrangements the technique could be adapted to flows in which the axial velocity profile variation is not principally in a single direction. A weight value theory for an electromagnetic flow meter with multiple electrodes has been implemented and proved to be a valid method for relating the mean flow velocity in a pixel to the potential differences measured between various pairs of electrodes. Moreover, this paper has used a matrix inversion method that can be combined with the weight values to reconstruct the mean velocity in each of a number of pixels from a given set of boundary potential difference measurements. In simulations, reconstructed velocities give good agreement with the reference pixel velocities and the reconstructed velocity profiles enable reasonably accurate volumetric flow estimates to be made. Experimental results for the measured water velocity profile, obtained in upward solids-in-water flows inclined at 0° and 30° to the vertical using a real multi-electrode electromagnetic flow meter, agreed well with the observed water velocity profile obtained from high speed filming. It is believed that the application of the techniques described in this paper to the measurement of highly non-uniform velocity profiles in multiphase flows is novel.

References

[1] Won Lim K, Chung MKyoon. Numerical investigation on the installation effects of electromagnetic flowmeter downstream of a 90° elbow–laminar flow case. Flow Measurement and Instrumentation 1999;10(3):167–74.
[2] Wang JZ, Tian GY, Lucas GP. Relationship between velocity profile and distribution of induced potential for an electromagnetic flow meter. Flow Measurement and Instrumentation 2007;18(2):99–105.
[3] Horner B. A novel profile-insensitive multi-electrode induction flowmeter suitable for industrial use. Measurement 1998;24(3):131–7.
[4] Xu LJ, Li XM, Dong F, Wang Y, Xu LA. Optimum estimation of the mean flow velocity for the multi-electrode inductance flowmeter. Measurement Science and Technology 2001;12:1139–46.

[5] Wang Mi, Ma Yixin, Holliday N, Dai Yunfeng, Williams RA, Lucas G. A high-performance EIT system. IEEE Sensors Journal 2005;5(2):289–99.
[6] Lijun Xu Ya, Wang, Dong Feng. On-line monitoring of nonaxisymmetric flow profile with a multielectrode inductance flowmeter. Instrumentation and Measurement, IEEE Transactions on 2004;53(4):1321–6.
[7] Williams EJ. The induction of electromotive forces in a moving liquid by a magnetic field, and its application to an investigation of the flow of liquids. Proceedings of the Physical Society 1930;42:466–78.
[8] Shercliff JA. the Theory of Electromagnetic Flow-Measurement. New Ed. Cambridge University Press; 1987.
[9] COMSOL Corporation Femlab 3.5a User Guide; 2005.
[10] Lucas GP, Cory J, Waterfall RC, Loh WW, Dickin FJ. Measurement of the solids volume fraction and velocity distributions in solids–liquid flows using dual-plane electrical resistance tomography. Flow Measurement and Instrumentation 1999;10(4):249–58.